Polythiophene Hybrids of Transition-Metal Bis(salicylidenimine)s: Correlation between Structure and Electronic Properties

Richard P. Kingsborough and Timothy M. Swager*

Contribution from the Department of Chemistry and Center for Material Science and Engineering, Massachusetts Institute of Technology, Cambridge, Massachusetts 02139

Received April 21, 1999

Abstract: The synthesis, electrochemistry, and spectroscopic behavior of tetradentate bis(salicylidenimine) transition metal complexes **5**−**9** are reported. Appending these complexes with 3,4-ethylenedioxythiophene (EDOT) moieties allows for electrochemical polymerization at much lower potentials than the parent salen complexes. The resulting polymers display well-defined organic-based electrochemistry at potentials <0.5 V vs Fc/Fc^+. The EDOT-modified *N*,*N*′-ethylene bis(salicylidene), *N*,*N*′-*o*-phenylene bis(salicylidene), and *N*,*N*′-*trans*-cyclohexylene bis(salicylidene) complexes **5a**−**b**, **6a**−**b**, and **8a**−**b** display cyclic voltammograms with four organic-based redox waves. Increasing the interchain separation through the use of nonplanar bis(salicylidene) ligands results in only two redox waves. The conductivity of the copper-based polymers decreases with increasing interchain spacing, with the maximum conductivity being 92 S cm^{-1} for poly(**5a**) and 16 S cm^{-1} for poly(**7a**). The nickel complexes were less sensitive to increased interchain separation and showed conductivities greater than 48 S cm^{-1} regardless of the interchain spacing and near 100 S cm^{-1} in the case of poly(**6b**). In situ spectroelectrochemistry was consistent with the segmented electronic nature of these polymers. Cyclic voltammetry of an analogous uranyl complex, **5c**, revealed that two electrons per repeat unit were removed during oxidation. Consideration of our collective investigations, which also included in situ EPR spectroscopic studies, led to a postulation that π-aggregation processes are occurring in those polymers which are allowed to have close interchain spacing.

Introduction

The incorporation of discrete transition metal complexes into conjugated polymeric systems has been the subject of extensive study.[1] Particular features of interest include a transition metal's ability to bind anions and small molecules (CO, O_2, NO, etc.),[2] or effect catalytic reactions.[3] The transport of electrons to the active metal center or the ability of the metal to affect the transport properties of the system are critical to generate useful materials. We have been interested in the incorporation of discrete transition metal complexes directly within a conducting polymer framework such that the metal center is intimately connected to the conduction pathway.[4,5] The design of these systems is based on a 2-fold hypothesis. The first is that we believe the ideal catalyst/sensory material will be realized when the metal-containing polymer functions as an extension of the electrode, mediating an activationless transfer of electrons from the base electrode to the electroactive metal centers. We also expect that changes at the metal center, e.g. binding events, will result in a modulation of the material's conductivity or optical properties.

Recently,[5] we have reported an *N*,*N*′-ethylenebis(salicylaldeniminato)cobalt(II)-based hybrid polymer in which the redox behavior of the metal complex and the organic scaffold was essentially amalgamated into a single entity. These initial results with redox-active metal centers have led us to investigate the differences between redox-active and redox-inactive metal centers. We are particularly interested in elucidating the role of the metal centers in the overall conduction pathways of these segmented polymers and what structural parameters govern their electrochemistry. By understanding these parameters, a rational design of electroactive sensory and catalytic materials can be undertaken.

Structures that incorporate transition metal salen complexes can give polymers that are electronically segmented in nature, that is, the intrachain conduction pathway is broken by the presence of the metal center. The segmented electronic nature of these metal-containing polymers can result in a number of interesting properties. One of these is a narrow window of high conductivity as a function of doping. Since conductivity in a segmented polymer will involve a dominance of interchain transport,[6,7] efficient communication between the isolated redox

(1) Kingsborough, R. P.; Swager, T. M. *Prog. Inorg. Chem.* **1999**, *48*, 123 and references therein.

(2) (a) Tovrog, B. S.; Drago, R. S. *J. Am. Chem. Soc.* **1974**, *96*, 6765. (b) Hoffman, B. M.; Szymanski, T.; Basolo, F. *J. Am. Chem. Soc.* **1975**, *97*, 637. (c) Cini, R.; Orioli, P. L. *J. Chem. Soc., Chem. Commun.* **1981**, 196. (d) Zanello, P.; Cini, R.; Cinquantini, A.; Orioli, P. L. *J. Chem. Soc., Chem. Commun.* **1983**, 2159.

(3) (a) *Handbook of Conducting Polymers*; Skotheim, T. A., Elsenbaumer, R. L., Reynolds, J. R., Eds.; Marcel Dekker: New York, 1998. (b) Audebert, P. *Curr. Top. Electrochem.* **1994**, *3*, 459. (c) Kelley, D. M.; Vos, J. G. In *Electroactive Polymer Electrochemistry*; Lyons, M. E., Ed.; Plenum: New York, 1994; Vol. 2. (d) Lyons, M. E. In *Electroactive Polymer Electrochemistry*; Lyons, M. E., Ed.; Plenum: New York, 1994; Vol. 1.

(4) (a) Zhu, S. S.; Swager, T. M. *Adv. Mater.* **1996**, *8*, 497. (b) Zhu, S. S.; Carroll, P. J.; Swager, T. M. *J. Am. Chem. Soc.* **1996**, *118*, 8713. (c) Zhu, S. S.; Swager, T. M. *J. Am. Chem. Soc.* **1997**, *119*, 12568.

(5) Kingsborough, R. P.; Swager, T. M. *Adv. Mater.* **1998**, *10*, 1100.

(6) (a) *Handbook of Conducting Polymers*; Skotheim, T. A., Ed.; Marcel Dekker: New York, 1986; Vols. 1 and 2. (b) *Conjugated Polymers*; Bredas, J. L., Silbey R., Eds.; Kluwer: Dordrecht, The Netherlands, 1991. (c) *Conjugated Polymers and Related Materials*; Salaneck, W. R., Lundstrom, I., Ranby, B., Eds.; Oxford University Press: Oxford, 1993.

(7) (a) Chung, T. C.; Kaufman, J. H.; Heeger, A. J.; Wudl, F. *Phys. Rev.* **1984**, *B30*, 702. (b) Heeger, A. J.; Kivelson, S.; Schrieffer, J. R.; Su, W. P. *Rev. Mod. Phys.* **1988**, *60*, 782.

10.1021/ja991285m CCC: $18.00 © 1999 American Chemical Society
Published on Web 09/09/1999

Scheme 1

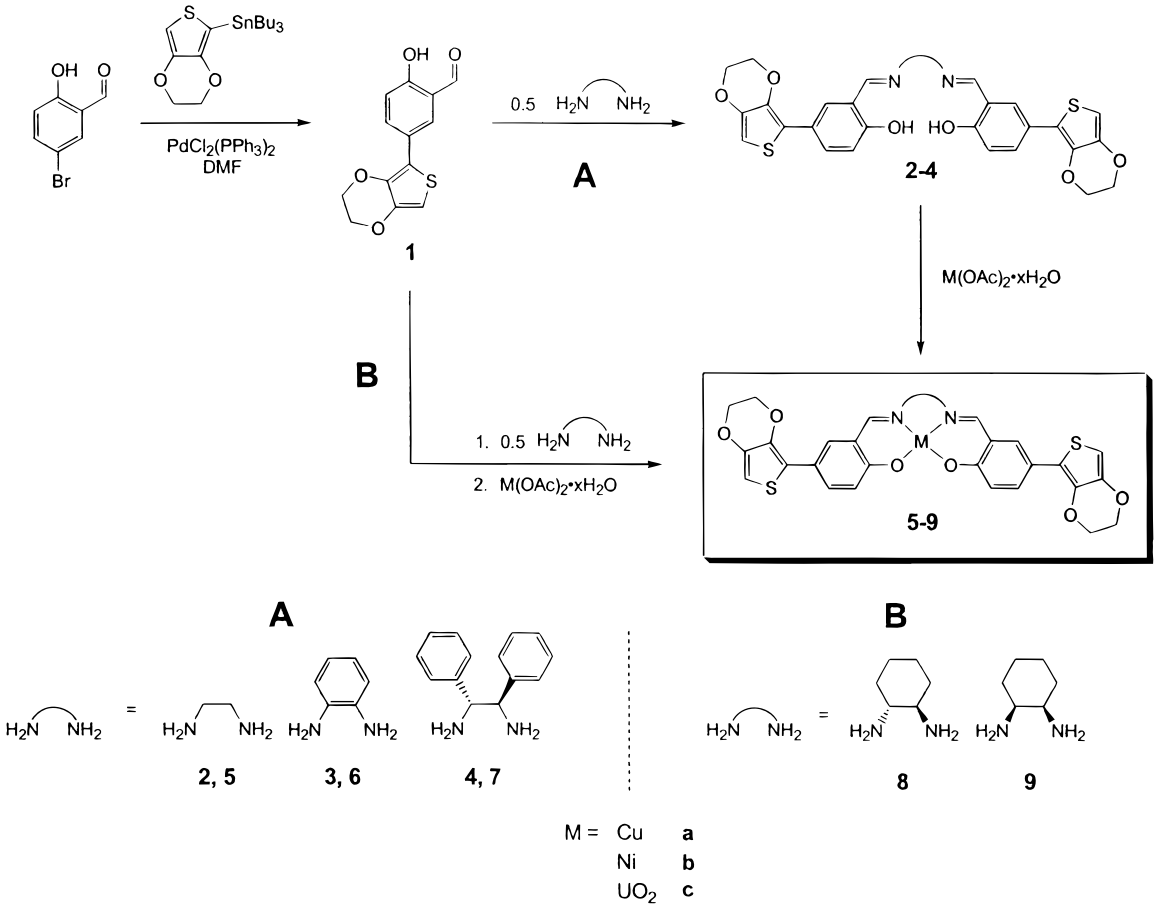

units in the polymer chains is expected for high conductivity. By using transition metals that are redox inactive over the potential range of the organic-based redox processes, correlations between the polymer structure and resulting electrochemistry can be made that are free from influences of metal-centered redox processes.

Our present work is concerned with the degree and nature of interactions between salen-type polymer chains (**I**). Chain−chain

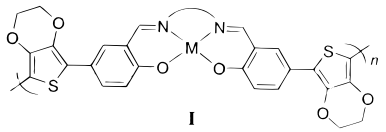

I

interactions have a number of ramifications but are best known for facilitating bulk conductivity and are generally necessary to display high conductivities.[6,7] Recent reports on oligomeric systems also implicate π-aggregation between conjugated polymer chains as an important component of these interactions.[8−10] In these aggregates, the polymers are in direct electronic communication with one another through weak, cofacial π-bonds between the aromatic rings. The presence of segmented structures appears to facilitate the formation of π-aggregates, probably by limiting the amount of delocalization. Such an effect has not been previously observed in segmented redox polymers incorporating transition metal centers in the main chain; however, these systems should also be prone to π-aggregate. In this contribution, we report systematic investigations of a series of coordinatively unsaturated 3,4-ethylenedioxythiophene-substituted bis(salicylaldenimine) copper, nickel, and uranyl complexes. In these studies, we have elucidated the role of interchain association by comparisons among a homologous series and a combination of cyclic voltammetry, square wave voltammetry, in situ UV−vis, EPR, and conductivity measurements as a function of applied electrochemical potential.

Results

Monomer Synthesis. The monomeric Schiff base complexes can be prepared by two separate routes depending on the diamine functionality, Scheme 1. The Schiff base ligands **2**−**4** were prepared in near quantitative yield by condensation of 2 equiv of **1**[5] with the appropriate diamine. Transition metal complexes **5**−**7**, with the exception of **6c**, were prepared in good to excellent yield by reacting ligands **2**−**4** with copper or nickel acetate in either DMF (**5a,b**) or refluxing methylene chloride/methanol (**5c**, **6a,b**, **7a,b**). Complexes **6c** and **8a,b** were prepared by first in situ preparation of the ligand in refluxing methylene chloride/methanol followed by addition of the metal acetate. Complexes **9a,b** were similarly prepared in warm ethanol. This one-pot method was employed since the free ligand could not be isolated cleanly. ^{1}H NMR of the diamagnetic species showed complete metal insertion. The purity of all of the metal complexes was confirmed by elemental analysis.

Monomer Electrochemical Polymerization. Saturated (ca. 0.1 mM) MeCN solutions of monomers **5a,b** are oxidatively polymerized when the potential of the electrode was swept between −0.6 and +0.4 V versus Fc/Fc$^+$ at a scan rate of 100

(8) Miller, L. L.; Mann, K. R. *Acc. Chem. Res.* **1996**, *29*, 417.
(9) Hong, Y.; Miller, L. L. *Chem. Mater.* **1995**, *7*, 1999.
(10) Hempenius, M. A.; Langeveld-Voss, B. M. W.; van Haare, J. A. E. H.; Janssen, R. A. J.; Sheiko, S. S.; Spatz, J. P.; Möller, M.; Meijer, E. W. *J. Am. Chem. Soc.* **1998**, *120*, 2798.

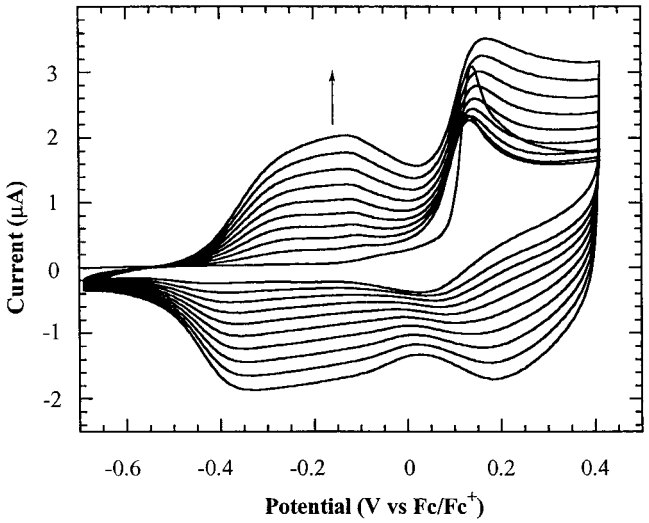

Figure 1. Anodic polymerization of **5a** at a 0.02 cm^2 Pt button electrode in 0.1 M Bu_4NPF_6/MeCN solutions at a scan rate of 100 mV/s.

mV/s.[11] A typical electrochemical polymerization of complex **5a** is shown in Figure 1. The first polymerization scan is characterized by a relatively sharp onset of monomer oxidation ($E_{onset,m}$) at +0.07 V followed by an associated reductive process ($E_{p,c}$) at +0.05 V on the return cycle. In subsequent potential sweeps, new oxidation waves grow in at −0.25 and −0.12 V. Repeated cycling results in further increased electroactivity of the electrode surface, indicative of polymer growth. On the basis of our earlier studies,[5] and the typical reaction paths of thiophene-containing monomers, polymers formed during the electrodeposition are proposed to have the structure shown in eq 1.

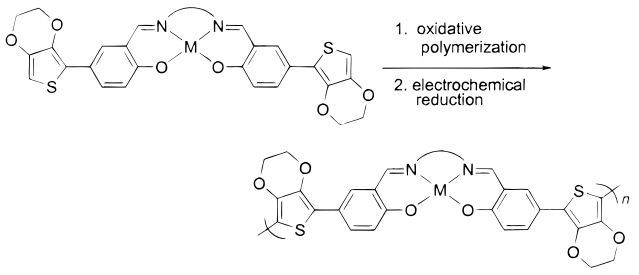

(1)

Polythiophene has been shown to follow a polymerization mechanism in which oxidized oligomers form as an insoluble precipitate on the electrode surface.[12] Typically after the initial deposition, the potential required for polymerization drops below the oxidation potential of the monomer, indicating that oxidized oligomers react with neutral thiophene monomers. The systems investigated herein are different and require application of the monomer oxidation potential to deposit polymer on the electrode surface during each potential sweep. Hence, cycling a thin polymer film of poly(**8a**) in a solution of fresh monomer from −0.6 to 0.1 V (ca. 200 mV less positive than for monomer oxidation) shows no growth of polymer. In addition, the polymer oxidation potential remains fixed throughout the polymerization process. All of these observations are in accord with the

(11) Unless noted all further potentials will be referenced versus this couple.

(12) (a) Leclerc, M.; Faïd, K. *Adv. Mater.* **1997**, *9*, 1087. (b) Roncali, J. *Chem. Rev.* **1992**, *92*, 711. (c) Wei, Y.; Chan, C.-C.; Tian, J.; Jang, G.-W.; Hseuh, K. F. *Chem. Mater.* **1991**, *3*, 888.

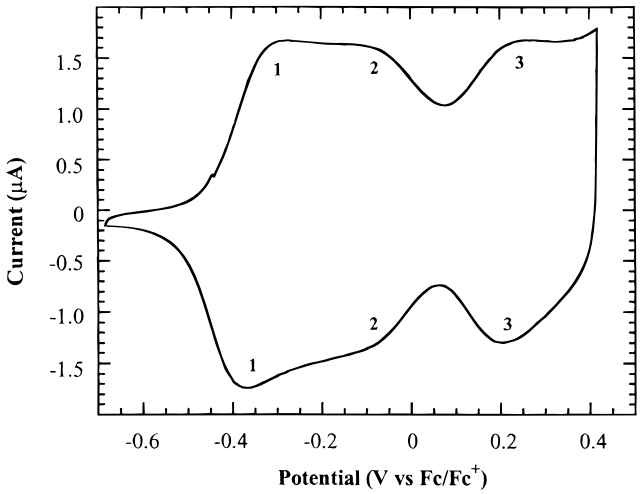

Figure 2. Cyclic voltammogram of poly(**5a**) highlighting the three-wave CV. Conditions are as in Figure 1.

segmented structure wherein the organic portion of the polymer has a short conjugation length that is interrupted by the metal binding sites. As a consequence, the terminal group of the growing polymer, which is likely oxidized to affect polymer growth, has nearly the same oxidation potential as the monomer.

Polymer Electrochemistry. The cyclic voltammogram (CV) of poly(**5a**) is shown in Figure 2. The CV is characterized by the appearance of three redox waves at −0.30, −0.06, and +0.27 V (Table 1). The first two redox waves overlap, while the wave at higher potential is well defined. These waves integrate in a 1:1:1 ratio; however, the ratio between the first and second waves is highly variable between samples. In these cases, the sum of the integrals of the first two waves is in a 2:1 ratio with the third. Examination of the CV of poly(**5c**) (Figure 3), in which the $U^{5+/6+}$ redox wave is completely separated from the organic potion of the CV, was used to determine the number of electrons oxidized per monomer unit. Integration of the organic-based redox waves versus the $U^{5+/6+}$ couple revealed that two electrons per repeat unit may be removed from the organic framework. This is in accordance with the expected most stable oxidized repeat unit structure in which the metal centers are bridged by the quinoid form of the repeat unit (Figure 4). Square-wave voltammetry was also used to help elucidate the electrochemistry displayed by poly(**5a**). The square-wave voltammogram, like the CV, yielded little definition within the broad redox wave at lower potentials, but a definite shoulder was seen at potentials corresponding to the first redox event. The second and third redox transitions possess much more defined peaks in the square-wave voltammogram.

The overall appearance of the CV for poly(**5a**) was found to be dependent on the solvent in which the polymer film was grown (Figure 5). Films grown in MeCN were found to have three waves in the CV. However, films grown in methylene chloride displayed a CV with only two waves integrating in a 1:1 relationship, which was also confirmed by square-wave voltammetry. To ascertain whether these differences can be attributed to a difference in polymer morphology, cyclic voltammograms of polymerized films were obtained in both solvents. In both cases, there was no change in the CV shape between the solvent in which the film was grown and the other solvent. For example, the CV of a polymer grown in MeCN still maintains three redox waves in CH_2Cl_2. Scanning electron microscopy images of the films grown in both acetonitrile and methylene chloride show substantially different morphologies.

Table 1. Cyclic Voltammetry and Conductivity Data

	cyclic voltammetry			conductivity	
polymer	$E_{p,a}$	$E_{p,c}$	ΔE	E_{max}[a]	σ (S cm^{-1})
5a	−0.25	−0.35	0.10	+0.51	92
	−0.11	−0.13	0.02		
	+0.25	+0.26	0.01		
	+0.56	+0.48	0.08		
5b	−0.29	−0.35	0.06	+0.51	77
	−0.08	−0.10	0.02		
	+0.27	+0.21	0.06		
5c	−0.83[b]	−0.92[b]	0.09	*c*	
	+0.19	+0.02	0.17		
	+0.37	+0.24	0.13		
6a	−0.19	−0.25	0.06	+0.46	90
	+0.04	−0.04	0.08		
	+0.41	+0.35	0.06		
	+0.69	+0.57	0.12		
6b	−0.26	−0.30	0.04	+0.46	99
	0.00	−0.01	0.01		
	+0.33	+0.29	0.04		
6c	−0.83[b]	−0.88[b]	0.05	*c*	
	+0.16	+0.08	0.08		
	+0.36	+0.33	0.03		
7a	−0.01	−0.11	0.10	+0.40	16
	+0.50	+0.32	0.18		
7b	−0.13	−0.18	0.05	+0.46	95
	+0.31	+0.28	0.03		
8a	−0.24	−0.35	0.11	+0.32	63
	+0.01	−0.13	0.14		
	+0.24	+0.21	0.03		
	+0.47	+0.32	0.15		
8b	−0.24	−0.35	0.11	+0.36	48
	−0.04	−0.13	0.09		
	+0.21	+0.19	0.03		
9a	−0.18	−0.37	0.19	+0.30	50
	+0.45	+0.30	0.15		
9b	−0.16	−0.20	0.04	+0.35	89
	+0.30	+0.27	0.03		

[a] Potential of maximum conductivity. [b] $U^{5+/6+}$ redox process. [c] No drain current detected.

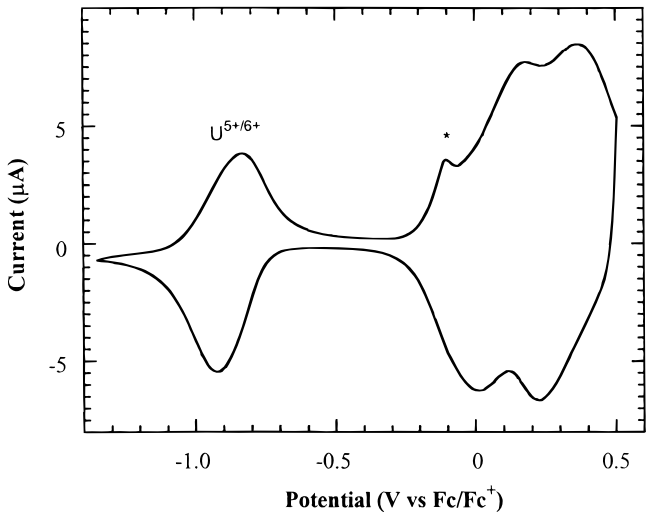

Figure 3. Cyclic voltammogram of poly(**5c**) showing the $U^{5+/6+}$ redox wave. The small shoulder at −0.1 V is due to a small amount of charge trapping (*). Conditions as in Figure 1.

Films grown in acetonitrile possess a rough texture, whereas films deposited in methylene chloride are fairly smooth and uniform.

Comparisons of the electrochemistry associated with **5a** and **5c** seem to suggest that significant chain-chain interactions play a role in determining the overall polymer electrochemistry. The four-coordinate copper complex enables short interchain distances, while the octahedral nature of the uranyl group prevents close approaches between polymer chains. To probe the structural parameters associated with polymers of this type, a homologous series of copper and nickel bis(salicylidenimine) complexes were prepared using diamine bridges of varying steric bulk. As both the copper and nickel Schiff base complexes display similar cyclic voltammetry, for brevity this discussion will be limited to principally the copper-based complexes. The cyclic voltammograms of copper-containing polymers **5**−**9** (Figure 6) show the interchain spacing to have a large effect. It is important to note that these polymers displayed limited stability at higher potentials (>0.5 V). However, sweeping to these high potentials, for example, in the case of poly(**5a**), revealed the existence of a fourth redox wave, such that the

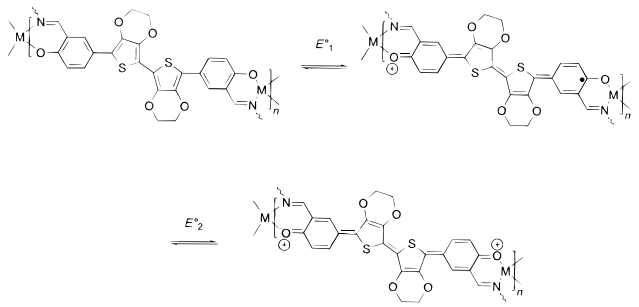

Figure 4. Variation of the polymer electronic structure with increasing oxidation potential.

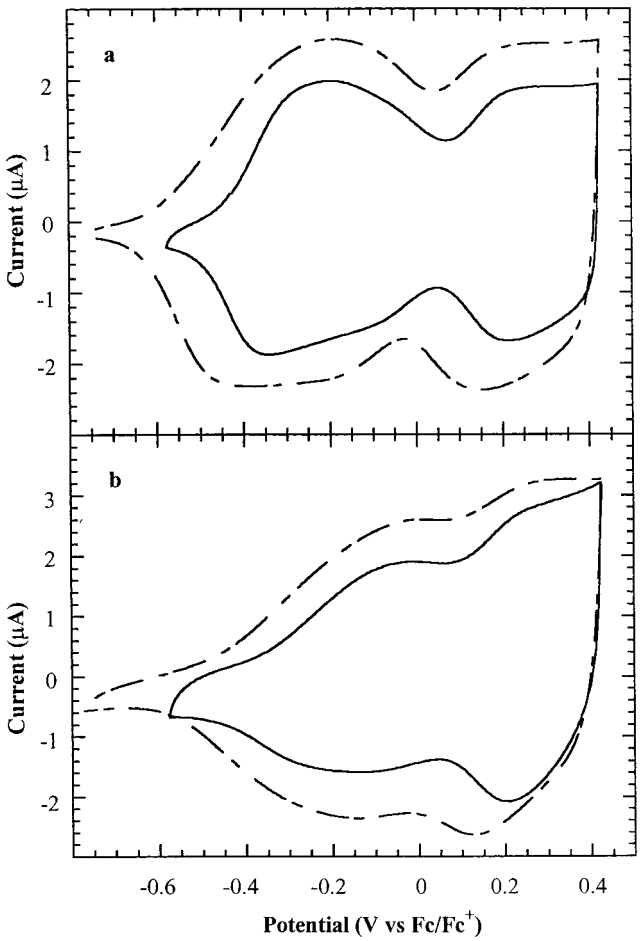

Figure 5. Cyclic voltammograms of poly(**5a**) showing the solvent dependence on the CV shape. (a) Polymer grown in MeCN: CV in MeCN (solid line), CV in CH_2Cl_2 (dashed line). (b) Polymer grown in CH_2Cl_2: CV in CH_2Cl_2 (dashed line), CV in MeCN (solid line). Conditions: 100 mV/s in 0.1 M Bu_4NPF_6.

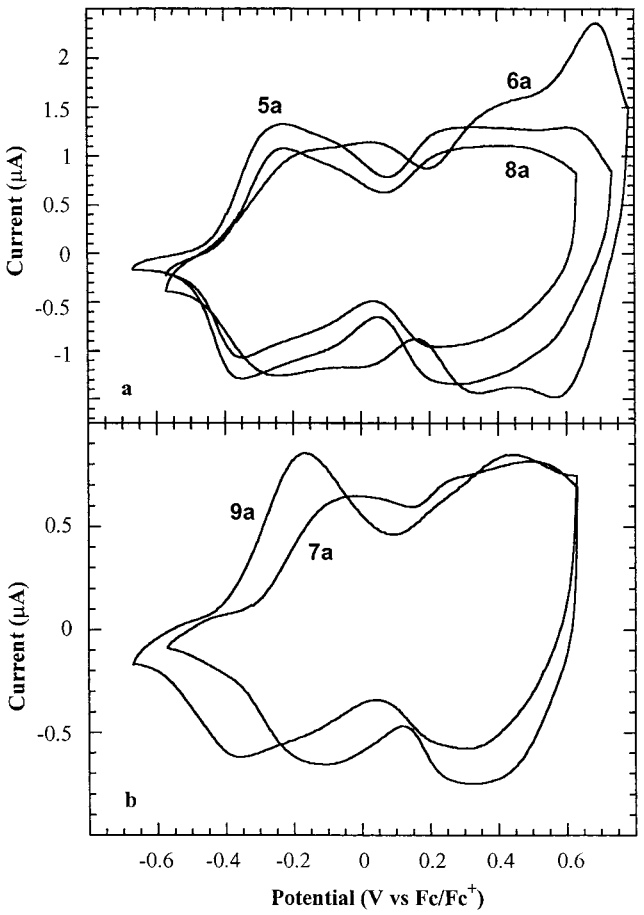

Figure 6. Cyclic voltammograms of poly(**5**−**9**) at a 0.02 cm^2 Pt button electrode in 0.1 M Bu_4NPF_6/MeCN solutions at a scan rate of 100 mV/s showing the variation of the CV shape with polymer structure.

polymer displayed four one-electron redox processes. Cycling the relatively planar polymers, such as poly(**5a**) and poly(**6a**), to ca. 0.7 V reveals the appearance of four redox waves. Complexes **7a** and **9a**, with more bulky diamine bridges to increase the interchain spacing in the polymer film, display only two waves in the polymer CV, even when heavily oxidized. Poly(**8a**) seems to be an intermediate case; a second redox wave at lower potentials is barely discernible.

The small interchain spacing expected for poly(**5**) and poly(**6**) favors a significant amount of interchain interactions. One manifestation of this interaction may be in the form of π-stacking. π-Stacking interactions between the chains have been observed previously in polymeric systems.[8,10,13−15] More extensive investigations into this phenomena have been carried out by Miller,[8,16] Janssen,[17] and others[13,18−19] using soluble, end-capped oligothiophenes and oligopyrroles, owing to their well-defined oligomer lengths, limited delocalization, and electrochemistry. These studies show that the dimerization equilibrium constant, K_{dim}, is both concentration and temperature dependent. In these polymer films the highly concentrated and relatively planar nature of the conducting polymer chains is expected to create a favorable environment for the formation of π-stacked polymeric structures.[8] π-Stacking interactions have also been implicated in the formation of mixed-valence $TTF_2^{+\bullet}$ dimers (TTF = tetrathiafulvalene) in TTF-substituted poly(bithiophene)s.[14] Dilution of the TTF species in the polymer by copolymerization with bithiophene reduced the intensity of this redox wave.

Complexes with 1,2-diphenylethylenediamine and the *cis*- and *trans*-1,2-diaminocyclohexane bridging units introduce substantially more steric bulk about the diamine bridge to prevent close contacts between polymer chains. Increasing the interchain distance tends to discourage π-aggregation, which has been observed by Zotti and co-workers in poly(dialkylcyclopentadithiophene)s.[13] In these systems, an increase in the length of the alkyl chain had a large effect on the shape of the CV as well as the ability of the chains to aggregate and form π-dimers, with long chains showing no π-dimerization.

Spectroelectrochemistry. Spectroelectrochemical measurements have been extensively used to observe the formation of π-dimers in both oligomeric species as and polymer matrices. The dimerization constants for oligomeric species in solution have been determined by following the growth or decrease of peak intensities associated with the monomeric and dimeric species. To probe the electronic nature of poly(**5**−**9**) and possibly observe the spectroscopic signature of a π-aggregation process, polymer films were grown on an indium tin oxide (ITO) coated glass slide electrode in a homemade three-electrode cell. The UV−vis−near-IR (NIR) spectra were then recorded as a function of oxidation potential. The yellow reduced film of poly(**5a**) is characterized by a transition centered at 430 nm. Upon being gradually stepped to the fully oxidized form, the polymers undergo a color change to dark blue. Figure 7a shows how the electronic absorptions of poly(**5a**) vary with applied potential. There is a rapid decrease in intensity of the high-energy absorption as the polymer begins to be oxidized, concurrent with the appearance of a new, lower energy absorption centered at 620 nm. Additionally, as the polymers approach their highest doping level, a band tailing into the NIR at lower doping levels begins to shift to higher energy. The NIR band has long been associated with the appearance of free carriers in the highly conductive state[20] and is often observed in purely organic conducting polymers.[20−22]

Films of poly(**7a**) display slightly higher energy transitions as compared to poly(**5a**), which is consistent with the higher oxidation potential of this polymer. The spectroscopic behavior of poly(**7a**) upon oxidation is similar to that of poly(**5a**) with the exception that at increased oxidation potentials (>0.3 V) a shoulder begins to grow in at 780 nm. At the same time, the

(13) Zotti, G.; Berlin, A.; Pagani, G.; Schiavon, G.; Zecchin, S. *Adv. Mater.* **1994**, *6*, 231.
(14) Huchet, L.; Akoudad, S.; Roncali, J. *Adv. Mater.* **1998**, *10*, 541.
(15) Yamamoto, T.; Komarudin, D.; Arai, M.; Lee, B.-L.; Suganuma, H.; Asakawa, N.; Inoue, Y.; Kubota, K.; Sasaki, S.; Fukuda, T.; Matsuda, H. *J. Am. Chem. Soc.* **1998**, *120*, 2047.
(16) (a) Graf, D. D.; Duan, R. G.; Campbell, J. P.; Miller, L. L.; Mann, K. R. *J. Am. Chem. Soc.* **1997**, *119*, 5888. (b) Hill, M. G.; Mann, K. R.; Miller, L. L.; Penneau, J. F. *J. Am. Chem. Soc.* **1992**, *114*, 2728. (c) Hill, M. G.; Penneau, J. F.; Zinger, B.; Mann, K. R.; Miller, L. L. *Chem. Mater.* **1992**, *4*, 1106. (d) Graf, D. D.; Campbell, J. P.; Miller, L. L.; Mann, K. R. *J. Am. Chem. Soc.* **1996**, *118*, 5480. (e) Miller, L. L.; Yu, Y.; Gunic, E.; Duan, R. *Adv. Mater.* **1995**, *7*, 547. (f) Yu, Y.; Gunic, G.; Zinger, B.; Miller, L. L. *J. Am. Chem. Soc.* **1996**, *118*, 1013.
(17) (a) van Haare, J. A. E. H.; Groenendaal, L.; Havinga, E. E.; Janssen, R. A. J.; Meijer, E. W. *Angew. Chem., Int. Ed. Engl.* **1996**, *35*, 638. (b) van Haare, J. A. E. H.; van Boxtel, M.; Janssen, R. A. J. *Chem. Mater.* **1998**, *10*, 1166.
(18) Faïd, K.; Leclerc, M. *Chem. Mater.* **1994**, *6*, 107.
(19) Bäuerle, P.; Segelbacher, U.; Maier, A.; Mehring, M. *J. Am. Chem. Soc.* **1993**, *115*, 10217.
(20) (a) Patil, A. O.; Heeger, A. J.; Wudl, F. *Chem. Rev.* **1988**, *88*, 183. (b) Chen, X.; Inganäs, O. *J. Phys. Chem.* **1996**, *100*, 15202.
(21) (a) Paul, E. W.; Ricco, A. J.; Wrighton, M. S. *J. Phys. Chem.* **1985**, *89*, 1441. (b) Thackeray, J. W.; White, H. S.; Wrighton, M. S. *J. Phys. Chem.* **1985**, *89*, 5133.
(22) See, for example: (a) Sotzing, G. A.; Reddinger, J. L.; Katritzky, A. R.; Soloducho, J.; Musgrave, R.; Reynolds, J. R. *Chem. Mater.* **1997**, *9*, 1578. (b) Soltzing, G. A.; Reynolds, J. R.; Steel, P. J. *Chem. Mater.* **1996**, *8*, 882.

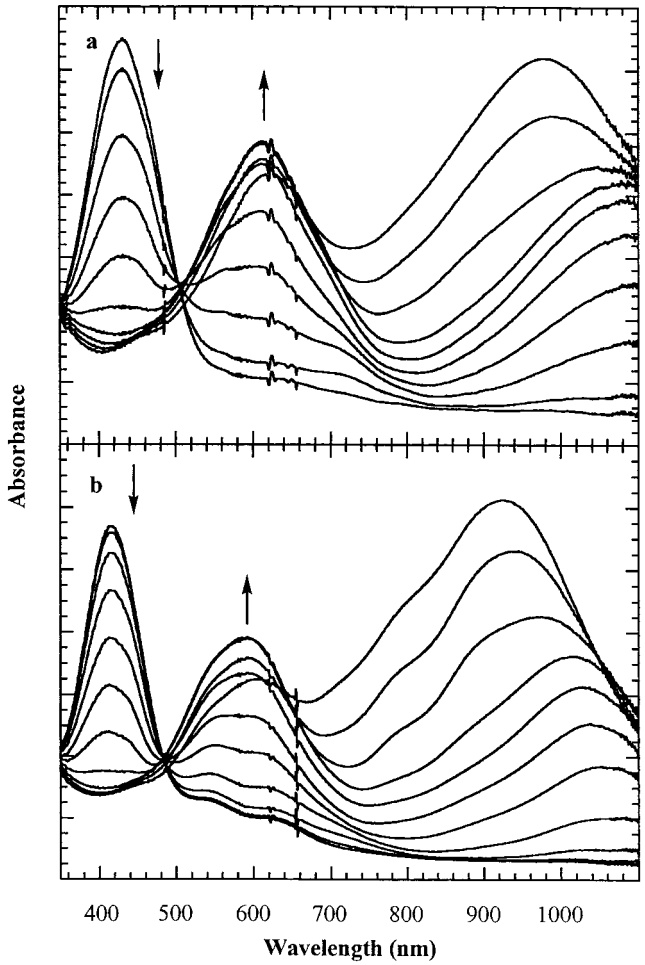

Figure 7. Electronic absorption measurements on ITO-coated glass as a function of oxidation potential for (a) poly(**5a**) (−0.3 to 0.6 V vs Fc/Fc^+), (b) Poly(**5c**) (−0.3 to 0.6 V vs Fc/Fc^+).

two peaks at 540 and 620 nm merge into one maximum at 580 nm. Again, at higher potentials (>0.4 V) there is a decrease in the intensity of this transition.

The sharpness of the transitions at 430 and 415 nm for poly(**5a**) and poly(**7a**), respectively, is indicative of the limited conjugation length in these systems (vide supra). In the reduced forms, these polymers have much higher energy $\pi-\pi^*$ transitions than in other organic-based conducting polymers.[13,22b,23] Upon oxidation, the relative sharpness of the transitions with respect to traditional conducting polymers is also indicative of the oligomeric, reduced conjugation length of these systems. The apparent similarities in the optical characteristics prevent any conclusions from being drawn as to the nature of chain aggregation.

In Situ EPR. In situ EPR spectroscopy has also been a very powerful technique used for the observation of π-dimerization processes.[13,16−17,22−25] An oligomer oxidized by a single electron shows a very characteristic EPR signal due to the presence of an unpaired electron in the π-system. Upon dimerization, a diamagnetic species is formed and the system becomes EPR silent.[13,16−17,24−25] We applied this technique to the nickel-containing representative polymers **5** and **7** to elucidate the spin states associated with the various redox waves. Films of the nickel-containing polymers were prepared on thin Pt wire electrodes and transferred to a flat cell quartz EPR tube along

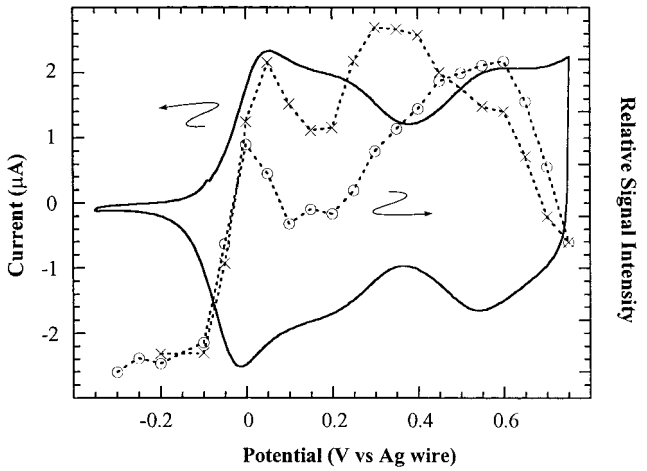

Figure 8. In situ EPR spectroscopy of films of poly(**5b**) grown on Pt wire electrodes. Solid line: cyclic voltammogram of poly(**5b**) on a Pt button electrode in 0.1 M Bu_4NPF_6/MeCN solutions at a scan rate of 100 mV/s. Dashed line: EPR signal intensity as a function of polymer oxidation potential in 50 mV potential steps (○, positive sweep; ×, negative sweep).

with a Pt wire counter electrode and a Ag wire reference electrode. The nickel complexes were investigated due to the similarity of the electrochemistry with the copper complexes and the metal center is EPR silent so that the only signals to be observed will be localized to the organic portion of the polymer.

Upon oxidation of poly(**5b**), a single EPR signal was observed at $g = 2.0038$ with a peak-to-peak separation of 10 G. At higher applied potentials, this signal shifted to $g = 2.027$ with a concurrent decrease in the peak-to-peak width to 6 G. Spin intensity data were determined at 50 mV steps after the polymer equilibrated for 2 min at that potential. The intensity of the EPR signal increased rapidly as the polymer was swept through the first oxidation potential (Figure 8), reaching a maximum at a potential slightly lower than the $E°_1$. This behavior is consistent with the formation of radical cations and has been observed in other conducting polymer systems.[26] Continued oxidation through $E°_2$ resulted in a decrease in the EPR signal intensity, suggesting the formation of π-aggregates. At higher potentials, the EPR intensity reached a global maximum. Data taken on the reverse scan indicate that this is a reversible process with some hysteresis being observed. It is interesting to note the higher spin count on the reverse scan as compared to the oxidative scan, presumably due to the dynamic processes occurring in the system, including solvation of the dicationic species and electrolyte migration out of the film.

Poly(**7b**) shows very different behavior compared to poly(**5b**) (Figure 9). The peak-to-peak width of the EPR signal ($g = 2.004$) remained constant at ca. 6 G as the polymer was oxidized. This allowed for a real-time measurement of the EPR signal intensity versus oxidation potential. Initial oxidation of the polymer results in a steep increase in the number of spin carriers in the polymer, much the same as poly(**5b**). Increasing the applied potential results in a rapid decrease of the signal intensity, with a small shoulder seen at 0.4 V vs Ag wire before

(23) Nowak, M. J.; Spiegel, D.; Hotta, S.; Heeger, A. J.; Pincus, P. A. *Macromolecules* **1989**, *22*, 2917.

(24) Zotti, G.; Schiavon, G.; Berlin, A.; Pagani, G. *Synth. Met.* **1993**, *61*, 81.

(25) Fajarí, Ll.; Brillas, E.; Alemán, C.; Juliá, L. *J. Org. Chem.* **1998**, *63*, 5324.

(26) (a) Chance, R. R.; Boudreaux, D. S.; Bredas, J. L.; Silbe, R. In *Handbook of Conducting Polymers*; Skotheim, T. A., Ed.; Marcel Dekker: New York, 1986; Vol. 2, pp 825−857 and references therein. (b) Bernier, P. In *Handbook of Conducting Polymers*; Skotheim, T. A., Ed.; Marcel Dekker: New York, 1986; Vol. 2, pp 1099−1125 and references therein.

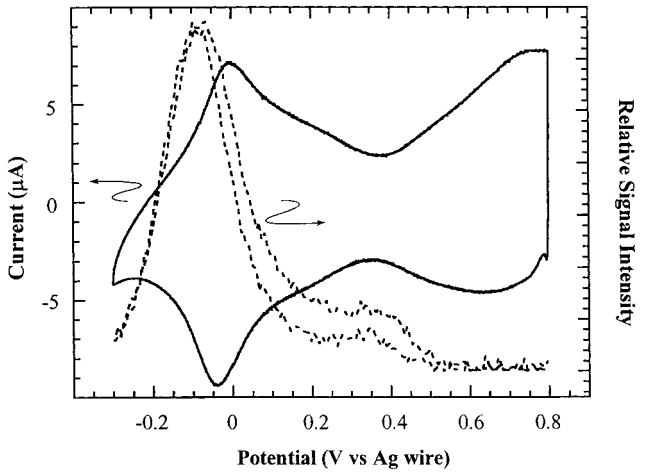

Figure 9. In situ EPR spectroscopy of films of poly(7**b**) grown on Pt wire electrodes. Solid line: cyclic voltammogram of poly(**7b**) on a Pt wire electrode in 0.1 M Bu_4NPF_6/MeCN solutions at a scan rate of 10 mV/s. Dashed line: EPR signal intensity as a function of polymer oxidation potential in a real-time measurement.

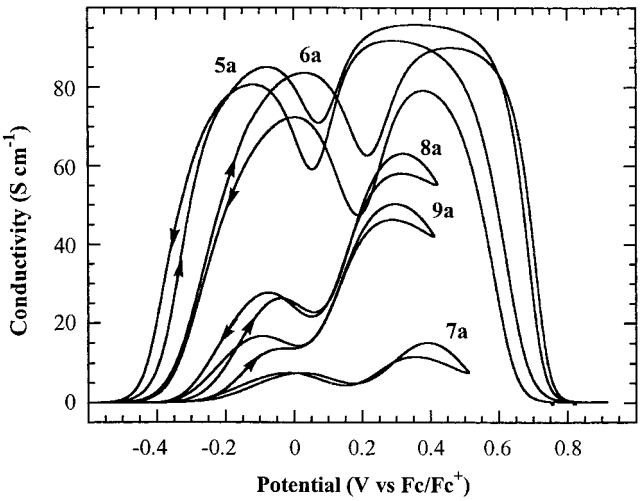

Figure 10. Conductivity versus polymer oxidation potential for the copper-containing polymer **5**−**9** on 5 μm interdigitated microelectrodes in 0.1 M Bu_4NPF_6/MeCN solutions at a scan rate of 2 mV/s with a 40 mV offset potential between the two working electrodes.

the signal intensity approaches zero at the polymer's highest oxidation potential (i.e. oxidation by two electrons per repeat unit), signifying that the majority of the charge carriers are spinless dications. Reversing the scan retraced the same path, with this behavior remaining constant during repeated scanning.

Conductivity Studies. The conductivity of these segmented polymers should be highly dependent on interchain processes.[6,7] To probe the conduction properties of these polymers as a function of chain spacing, we utilized methods developed by Wrighton and co-workers[21,27] to investigate polymer conductivity as a function of oxidation potential. Polymer films were electrochemically deposited on 5 μm interdigitated microelectrodes such that the film connected the two sets of electrodes. After a small potential difference (V_D) was applied between the two electrodes, typically 40 mV, both electrodes were scanned versus the reference electrode at a slow scan rate (2 mV/s). The drain current (i_D) that flowed between the two sets of electrodes, source and drain, is then observed as a function of the applied potential, Figure 6. This drain current can be related directly to absolute conductivity (σ) by eq 2,

$$\sigma = \frac{i_D}{V_D}\frac{W}{nTL} \qquad (2)$$

where W is the distance between the electrodes (5 μm), n is the number of spaces between electrodes, T is the thickness of the film in the region between the electrodes as measured by profilometry, and L is the length of the finger.[28]

The polymer conductivities are summarized in Table 1. The copper-based polymers poly(**5a**) and poly(**6a**) display rapid increases in conductivity upon initial polymer oxidation followed by a subsequent decrease in conductivity after passing the second oxidation wave (Figure 10). Increasing the potential through the third oxidation wave results in a further increase in conductivity and eventually the conductivity reaches a plateau with conductivities near 90 S cm^{-1}. This bimodal conductivity profile is consistent with the segmented nature of the polymer backbone and has been observed previously in bipyridine-containing hybrid systems.[4] Further oxidation of the polymer to 1.0 V, whereat the polymer is oxidized by a full 2 electrons per repeat unit, results in a rapid decrease of the conductivity starting at approximately 0.8 V. The polymers had limited stability at these high oxidation states which prevented EPR and optical studies from being conducted. The reverse scans, from 0.5 or 1.0 V, show some hysteresis, consistent with that observed for other polymers.[21,27] Some degradation of conductivity is observed after repeated scans to 1.0 V; little loss of conductivity with multiple scans is seen when reversing the sweep at 0.5 V. As was the case with the cyclic voltammetry, perturbations of the interchain distance have profound effects on the polymer conductivity profile. As seen in Figure 10, increasing the steric bulk of the diamine bridge results in a drop in conductivity in the order **8a** > **9a** > **7a**. The conductivity of a film of poly(**5a**) grown in methylene chloride displayed a conductivity profile consistent with weakly interacting chains, similar to poly(**7a**).

The nickel-based polymers, unlike their copper analogues, appear to have conductivities that are somewhat insensitive to the sterics of the complexes (Table 1). All of the polymers, with the exception of **8b**, display high conductivities when fully oxidized, reaching a plateau trace similar to that of the copper polymers **5a** and **6a**. Poly(**8b**) displays a conductivity trace analogous to poly(**8a**) in that the conductivity reaches a global maximum and then immediately begins to decrease. We can speculate that the differences between the copper and nickel systems may be due to both the rigid square-planar nature of the nickel complexes as well as a d_{z^2} frontier orbital. In this molecular orbital arrangement, there is sufficient electron density sticking out of the plane of the complex that there may be overlap with the nickel center of another polymer chain, thus facilitating electron hopping between chains. For comparison, in polymers based on thiochelated transition metal complexs,[1] the nickel complexes of a wide variety of structural motifs generally show greater conductivity values than their copper counterparts, thus implicating the role of metal orbital overlap as a viable conduction pathway.

(27) (a) Kittlesen, G. P.; White, H. S.; Wrighton, M. S. *J. Am. Chem. Soc.* **1984**, *106*, 7389. (b) Ofer, D.; Crooks, R. M.; Wrighton, M. S. *J. Am. Chem. Soc.* **1990**, *112*, 7869.

(28) Conductivity measurements are referenced to poly(3-methylthiophene) (σ = 60 S cm^{-1}),[29] similar to experiments performed by Zotti and co-workers: Zotti, G.; Schiavon, G. *Synth. Met.* **1990**, *39*, 183. Schiavon, G.; Sitran, S.; Zotti, G. *Synth. Met.* **1989**, *32*, 209. This method was verified by determining the conductivity of poly(EDOT) under the same conditions, which we found to be 110 S cm^{-1}, which is only a factor of 2 lower than the value reported in the literature for electrochemically grown material: Heywang, G.; Jonas, F. *Adv. Mater.* **1992**, *4*, 116.

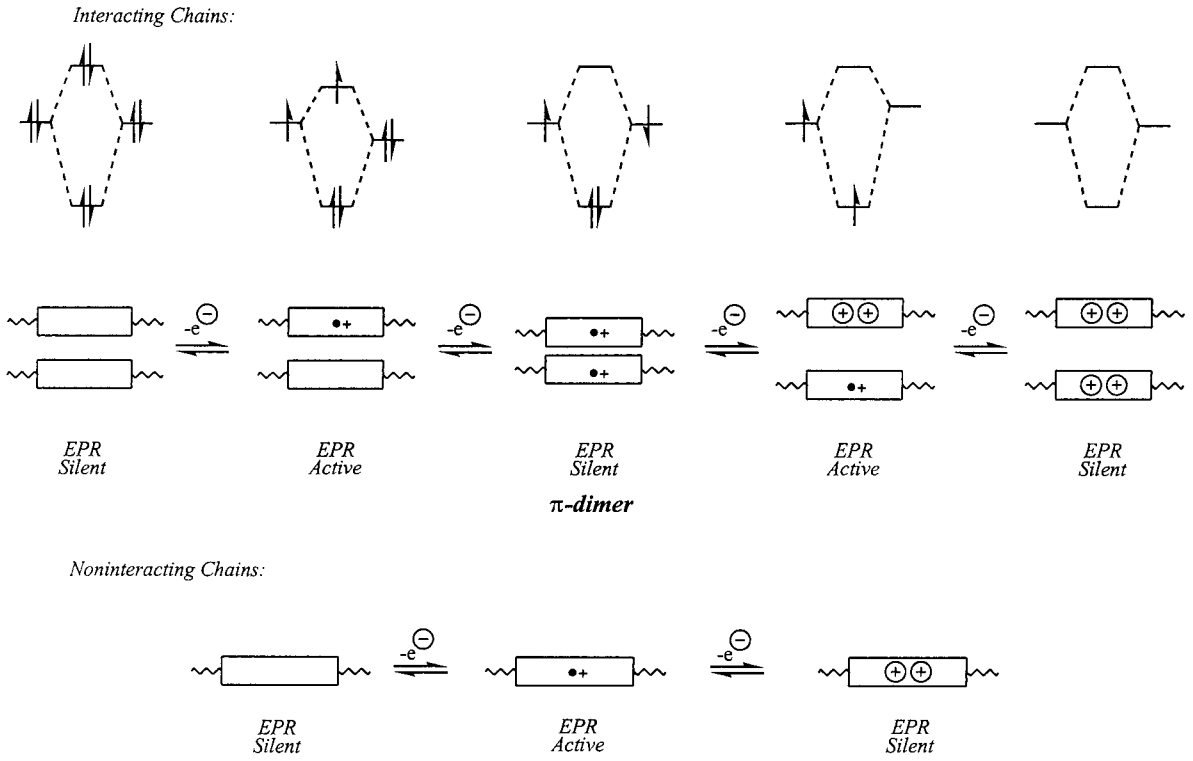

Figure 11. Summary of the possible electrochemical processes occurring in poly(**5**−**9**) taking into account the segmented nature of these polymers.

Discussion

From these data, one can envision two different electrochemical processes taking place in these polymers, as schematically illustrated in Figure 11. In these segmented polymers, both UV−vis and the polymerization mechanism reveal short conjugation lengths. For simplicity, we will consider interactions between the isolated redox units of different chains in close proximity to one another. In cases where there are large chain−chain interactions, and an interacting chain scheme (Figure 11, top) dominates, we see a lower oxidation potential consistent with a destabilizing interaction between the HOMOs. EPR data from poly(**5**) suggest that initial oxidation produces radical cations. Further oxidation of the electron in the pseudo-π* orbital creats a spin-paired species (π-dimer). Continued oxidation at higher potentials removes an electron from this dimeric species to result in an unpaired spin, and at the highest potential a dicationic, EPR-silent species is observed.

The noninteracting chains are found, as expected, to display a much simpler electrochemistry (Figure 11, bottom). Oxidation of the polymer film creates radical cations, which are subsequently oxidized to dications at the second oxidation potential. The highly variable nature of the cyclic voltammetry for poly(**5**) and poly(**8**) is the result of the disordered nature of the polymer films. In these cases, the observed electrochemistry can be a combination of both interacting and noninteracting redox units.

Concluding Remarks

The nature of the polymer electrochemistry for the copper and nickel complexes **5**−**9** is greatly influenced by interchain spacing. It has been shown that we can modulate this interchain interaction through the introduction of additional steric bulk on the diamine bridging group yet still retain desirable electrochemical properties (stability, high conductivity). Control of the metal coordination sphere is essential to development of chemoresistive sensors as well as electrocatalytic materials. Understanding the design parameters for this class of conducting polymers and how these parameters control the electrochemical properties will greatly assist in choosing starting points for the development of active catalysts. Currently we are investigating both these and related materials for the development of solution and vapor-phase chemoresistive sensors and for various electrocatalytic applications such as dioxygen reduction.

Experimental Section

General Methods. NMR spectra (^{1}H and ^{13}C) were obtained on Bruker AC-250, Varian Mercury-300, or Varian Inova-500 MHz spectrometers. Chemical shifts are reported in ppm relative to Me_4Si (^{1}H) or residual protio solvent (^{13}C). Elemental analyses were performed by Desert Analytics, Tucson, AZ. Mass spectra were obtained at the MIT instrument center. IR spectra were recorded as KBr pellets on a Nicolet Impact 410 spectrophotometer. UV−vis spectra were recorded on a Hewlett-Packard 8453 diode array spectrophotometer.

Materials. Synthetic manipulations requiring an inert atmosphere were performed under argon in oven-dried glassware using standard Schlenk techniques or in an Innovative Technologies drybox. DMF was purchased from Aldrich as a sure-seal bottle and used as received. MeCN was purchased from Aldrich as a sure-seal bottle and stored over activated alumina. Ethylenediamine, 1,2-phenylenediamine, (1*R*,2*R*)-(+)-1,2-diphenylethylenediamine, (1*R*,2*R*)-(+)-1,2-diaminocyclohexane, and *cis*-1,2-diaminocyclohexane were purchased from Aldrich and used as received. 2-Tributylstannyl-3,4-ethylenedioxythiophene was prepared by literature methods and purified by distillation.[4c] 5-(2-(3,4-Ethylenedioxy)thienyl)salicylaldehyde (**1**) and *N*,*N*′-ethylenebis(5-(2-(3,4-ethylenedioxy)thienyl)salicylidenimine) (**2**) were prepared by methods described previously.[5]

Caution: Care should be taken when handling uranyl-containing compounds because of their toxicity and radioactivity.[30]

Ligand 3. To a suspension of 252 mg (0.961 mmol) of 5-(2-(3,4-ethylenedioxy)thienyl)salicylaldehyde in 15 mL of ethanol was added 1,2-phenylenediamine (52 mg, 0.480 mmol, 0.50 equiv) with continued

(29) Tourillon, G.; Garnier, G. *J. Electroanal. Chem.* **1982**, *135*, 173.
(30) *Dangerous Properties of Industrial Materials*, 5th ed.; Sax, N. I., Ed.; van Nostrand Reinhold Company: New York, 1979; pp 1078−1079.

stirring and the mixture was heated to 60 °C. After 1 h, the reaction was cooled to room temperature and the resulting red solid was filtered, washed with ethanol, and dried in vacuo to afford 126 mg of product. An additional 46 mg of product was recovered by recrystallizing the filtrate for an overall yield of 172 mg (0.288 mmol, 60%) of red solid (mp 200−202 °C dec). ^{1}H NMR (500 MHz, $CDCl_3$) δ 13.10 (s, 2H), 8.69 (s, 2H), 7.75 (d, 2H, J = 2.5 Hz), 7.71 (dd, 2H, J = 8.8 and 2.5 Hz), 7.36 (dd, 2H, J = 5.8 and 3 Hz), 7.28 (dd, 2H, J = 6 and 3.5 Hz), 7.07 (d, 2H, J = 8.5 Hz), 6.25 (s, 2H), 4.31−4.24 (m, 8H). The poor solubility of this compound prevented characterization by ^{13}C NMR. IR (KBr) 1619 cm^{-1}. MS m/z 597 ([M + H]$^+$). HRMS (FAB) found m/z 596.1070 (M$^+$); calcd for $C_{32}H_{24}N_2O_6S_2$ (M$^+$) 596.1076. Elemental Anal. calcd for $C_{32}H_{24}N_2O_6S_2$: C, 64.41; H, 4.05; N, 4.69. Found: C, 63.52; H, 3.58; N, 4.44.

Ligand 4. This compound was prepared in a fashion similar to **3** with a yield of 69% yellow solid, mp 208−210 °C. ^{1}H NMR (500 MHz, $CDCl_3$) δ 13.39 (s, 2H), 8.35 (s, 2H), 7.60 (dd, 2H, J = 8.8 and 2.5 Hz), 7.51 (d, 2H, J = 2 Hz), 7.24−7.18 (m, 10H), 6.97 (d, 2H, J = 9 Hz), 6.20 (s, 2H), 4.76 (s, 2H), 4.26−4.20 (m, 8H). ^{13}C NMR (126 MHz, $CDCl_3$) δ 166.4, 160.0, 142.3, 139.5, 137.4, 130.8, 129.5, 128.6, 128.0, 127.9, 124.5, 118.7, 117.5, 116.9, 96.6, 80.4, 64.9, 64.7. IR (KBr) 1629 cm^{-1}. MS m/z 700 (M$^+$). HRMS (FAB) found m/z 700.1705 (M$^+$); calcd for $C_{40}H_{32}N_2O_6S_2$ m/z 700.1702 (M + H$^+$). Elemental Anal. calcd for $C_{40}H_{32}N_2O_6S_2$: C, 68.55; H, 4.60; N, 4.00. Found: C, 68.22; H, 4.73; N, 3.71.

General Procedure for 5a,b. To a slurry of **2** in DMF was added 1.1 equiv of metal acetate with continued stirring. The reaction was allowed to stir at room temperature overnight, after which time the solvent was evaporated. The solid was washed with methanol and dried under vacuum to afford the desired complex.

Complex 5a: 54% olive green solid, mp >250 °C dec. IR (KBr) 1628 cm^{-1}. MS m/z 610 (M$^+$). HRMS (FAB) found m/z 610.0293 ([M + H]$^+$); calcd for $C_{28}H_{22}CuN_2O_6S_2$ ([M + H]$^+$) 610.0294. Elemental Anal. calcd for $C_{28}H_{24}CuN_2O_7S_2$: C, 53.54; H, 3.85; N, 4.46. Found: C, 53.09; H, 3.42; N, 4.44.

Complex 5b: 91% reddish brown solid, mp >250 °C dec. ^{1}H NMR (DMF, 250 MHz) δ 8.05 (s, 2H), 7.64 (d, 2H, J = 2.4 Hz), 7.59 (dd, 2H, J = 1.9 and 8.9 Hz), 6.79 (d, 2H, J = 8.8 Hz), 6.46 (s, 2H), 4.36−4.29 (m, 8H), 3.58 (s, 4H). ^{13}C NMR (DMSO, 125 MHz) δ 164.1, 163.3, 142.9, 137.3, 131.9, 129.7, 121.0, 120.6, 120.5, 116.8, 95.7, 65.2, 64.8, 58.8. IR (KBr) 1620 cm^{-1}. MS m/z 605 ([M + H]$^+$). HRMS (FAB) found m/z 605.0352 (M$^+$); calcd for $C_{28}H_{22}N_2NiO_6S_2$ ([M + H]$^+$) 605.0351. Elemental Anal. calcd for $C_{28}H_{22}N_2NiO_6S_2$: C, 55.56; H, 3.66; N, 4.63. Found: C, 55.05; H, 3.72; N, 4.80.

Complex 5c. To a yellow slurry of 111 mg (0.202 mmol) of **2** in 12 mL of CH_2Cl_2 and 3 mL of MeOH was added 86 mg (0.202 mmol) of $UO_2(OAc)_2\cdot 2H_2O$ with continued stirring. The reaction quickly turned red and the solution was heated to reflux overnight. The reaction was cooled to room temperature and filtered. The rust colored solid was washed with MeOH and dried under vacuum to afford 138 mg (0.165 mmol, 82%) of rust colored powder (mp >250 °C dec). ^{1}H NMR (DMSO, 250 MHz) δ 9.54 (s, 2H), 7.89−7.85 (m, 4H), 6.99 (d, 2H, J = 8.4 Hz), 6.49 (s, 2H), 4.52 (s, 4H), 4.36−4.29 (m, 8H). ^{13}C NMR (DMSO, 125 MHz) δ 168.8, 168.0, 142.1, 137.0, 132.3, 131.3, 13.7, 121.3, 121.0, 116.0, 96.0, 64.7, 64.2, 63.7. IR (KBr) 1623 cm^{-1}. MS m/z 817 ([M + H]$^+$). HRMS (FAB) found m/z 817.1401 ([M + H]$^+$); calcd for $C_{28}H_{22}N_2O_8S_2U$ ([M + H]$^+$) 817.1404. Elemental Anal. calcd for $C_{28}H_{22}N_2O_8S_2U$: C, 41.18; H, 2.72; N, 3.43. Found: C, 41.83; H, 2.78; N, 3.32.

General Procedure for 6a,b and 7a,b. To a yellow solution of the ligand in 10 mL of CH_2Cl_2 and 5 mL of MeOH was added 1.1 equiv of the appropriate metal acetate with continued stirring. The reaction was stirred at reflux or 12 H, after which time the solvent volume was reduced. The resulting precipitate was washed with MeOH and dried under vacuum to afford the desired complex.

Complex 6a: 97% of red-orange solid, mp >250 °C. IR (KBr) 1613 cm^{-1}. MS m/z 658 ([M + H]$^+$). HRMS (FAB) found m/z 657.0211 (M$^+$); calcd for $C_{32}H_{22}CuN_2O_6S_2$ (M$^+$) 658.0315. Elemental Anal. calcd for $C_{32}H_{22}CuN_2O_6S_2\cdot H_2O$: C, 56.84; H, 3.58; N, 4.14. Found: C, 56.38; H, 2.63; N, 3.95.

Complex 6b: 90% red-orange solid, mp >250 °C. ^{1}H NMR (300 MHz, DMSO-d_6) δ 9.08 (s, 2H), 8.21 (dd, 2H, J = 3.6 and 6 Hz), 7.89 (d, 2H, J = 2.1 Hz), 7.68 (dd, 2H, J = 2.4 and 9 Hz), 7.36 (dd, 2H, J = 3 and 6.2 Hz), 6.95 (d, 2H, J = 9 Hz), 6.51 (s, 2H), 4.32−4.23 (m, 8H). The poor solubility of this compound prevented characterization by ^{13}C NMR. IR (KBr) 1614 cm^{-1}. MS m/z 653 ([M + H]$^+$). HRMS (FAB) found m/z 652.0262 (M$^+$); calcd for $C_{32}H_{22}N_2NiO_6S_2$ (M$^+$) 652.0273. Elemental Anal. calcd for $C_{32}H_{22}N_2NiO_6S_2$: C, 58.83; H, 3.39; N, 4.29. Found: C, 58.33; H, 3.02; N, 4.15.

Complex 7a: 83% green-brown solid, mp >250° dec. IR (KBr) 1628 cm^{-1}. MS m/z 762 ([M + H]$^+$). HRMS (FAB) found m/z 761.0839 (M$^+$); calcd for $C_{40}H_{30}CuN_2O_6S_2$ 762.0920 ([M + H]$^+$). Elemental Anal. calcd for $C_{40}H_{30}CuN_2O_6S_2$: C, 63.02; H, 3.97; N, 3.67. Found: C, 62.33; H, 3.34; N, 3.45.

Complex 7b: 89% green-brown solid, mp >250° dec. ^{1}H NMR (500 MHz, $CHCl_3$) δ 7.90 (d, 4H, J = 7.5 Hz), 7.59 (dd 2H, J = 8.8 and 2.5 Hz), 7.46 (t, 4H, J = 7 Hz), 7.38 (t, 2H, J = 7 Hz), 7.36 (s, 2H), 7.32 (d, 2H, J = 2 Hz), 7.11 (d, 2H, J = 9 Hz), 6.14 (s, 2H), 4.50 (s, 2H), 4.21−4.17 (m, 8H). ^{13}C NMR (125 MHz, $CHCl_3$) δ 164.6, 163.7, 142.3, 139.8, 136.8, 133.2, 129.6, 129.5, 127.5, 122.4, 121.0, 120.2, 117.3, 95.9, 79.8, 64.8, 64.7. IR (KBr) 1614 cm^{-1}. MS m/z 757 ([M + H]$^+$). HRMS (FAB) found m/z 756.0896 (M$^+$); calcd for $C_{40}H_{30}N_2NiO_6S_2$ 757.0977 ([M + H]$^+$). Elemental Anal. calcd for $C_{40}H_{30}N_2NiO_6S_2$: C, 63.42; H, 3.99; N, 3.70. Found: C, 63.01; H, 3.74; N, 3.52.

Complex 6c. To a solution of **1** (99 mg, 0.377 mmol) in 15 mL of methylene chloride was added 1,2-phenylenediamine (20 mg, 0.189 mmol, 0.5 equiv). The yellow solution was refluxed for 30 min and then 80 mg (0.189 mmol, 0.5 equiv) of $UO_2(OAc)_2\cdot 2H_2O$ and 5 mL of methanol were added. The red solution was refluxed for an additional 1 h, after which time the solvent volume was reduced and complex precipitation was induced by dropwise addition of petroleum ether. The red-orange product was filtered, washed with petroleum ether, and dried under vacuum to yield 130 mg (0.150 mmol, 79%) of red-orange solid (mp >250 °C). ^{1}H NMR (500 MHz, DMSO-d_6) δ 9.70 (s, 2H), 8.07 (d, 2H, J = 2.5 Hz), 7.93 (dd, 2H, J = 2 and 8.5 Hz), 7.85 (dd, 2H, J = 3.5 and 5.8 Hz), 7.56 (dd, 2H, J = 3.5 and 6.3 Hz), 7.05 (d, 2H, J = 8.5 Hz), 6.49 (s, 2H), 4.30−4.23 (m, 8H). ^{13}C NMR (125 MHz, DMSO-d_6) δ 168.7, 166.8, 146.6, 142.1, 137.3, 133.7, 132.5, 129.0, 124.2, 122.0, 121.1, 120.6, 115.7, 99.0, 96.3, 64.7, 64.2. IR (KBr) 1611 cm^{-1}. MS m/z 865 ([M + H]$^+$). HRMS (FAB) found m/z 864.1309 (M$^+$); calcd for $C_{32}H_{22}N_2O_8S_2U$ ([M + H]$^+$) 865.1404. Satisfactory elemental analysis could not be obtained for this complex after multiple attempts.

Complex 8a. To a solution of 116 mg (0.442 mmol) of **1** in 8 mL of CH_2Cl_2 and 4 mL of MeOH was added 25 mg (0.221 mmol, 0.5 equiv) of (1*S*,2*S*)-diaminocyclohexane with continued stirring. The yellow solution was refluxed for 1 h, and then 49 mg (0.243 mmol, 0.55 equiv) of $Cu(OAc)_2\cdot H_2O$ was added to result in a red-brown precipitate. The reaction was refluxed for 1 h and cooled to room temperature. Filtration of the solid, followed by washing with MeOH and drying under vacuum yielded 119 mg (0.179 mmol, 81%) of dark gold solid (mp >250 °C). IR (KBr) 1628 cm^{-1}. MS m/z 664 ([M + H]$^+$). HRMS (FAB) found m/z 663.0675 (M$^+$); calcd for $C_{32}H_{28}CuN_2O_6S_2$ ([M + H]$^+$) 664.0763. Elemental Anal. calcd for $C_{32}H_{28}CuN_2O_6S_2\cdot H_2O$: C, 56.33; H, 4.43; N, 4.11. Found: C, 56.71; H, 4.15; N, 3.95.

Complex 8b. This complex was prepared by similar procedures except using $Ni(OAc)_2\cdot 4H_2O$ to yield 92% dark gold solid, mp >250 °C. ^{1}H NMR (300 MHz, $CDCl_3$) δ 7.45 (dd, 2H, J = 2.4 and 9 Hz), 7.30 (d, 2H, J = 2.4 Hz), 7.28 (s, 2H), 6.91 (d, 2H, J = 8.7 Hz), 6.04 (s, 2H), 4.15−4.08 (m, 8H), 3.05 (br, 2H), 2.33 (br, H), 1.82 (br, 2H), 1.23 (br, 4H). The poor solubility of this compound prevented characterization by ^{13}C NMR. IR (KBr) 1618 cm^{-1}. MS m/z 659 ([M + H]$^+$). HRMS (FAB) found m/z 658.0738 (M$^+$); calcd for $C_{32}H_{28}N_2NiO_6S_2$ ([M + H]$^+$) 659.0821. Elemental Anal. calcd for $C_{32}H_{28}N_2NiO_6S_2$: C, 58.29; H, 4.28; N, 4.25. Found: C, 57.41; H, 3.95; N, 4.91.

Complex 9a. To a solution of 88 mg (0.336 mmol) of **1** in 10 mL of EtOH was added 20 μL (0.168 mmol, 0.5 equiv) of *cis*-1,2-diaminocyclohexane with continued stirring. The suspension was heated

at 50 °C for 1 h, and then 37 mg (0.185 mmol, 0.55 equiv) of $Cu(OAc)_2 \cdot H_2O$ was added to result in a red-brown precipitate. The reaction was refluxed for 1 h and cooled to room temperature. Filtration of the solid, followed by washing with EtOH and drying under vacuum yielded 91 mg (0.137 mmol, 82%) of brown solid (mp >250 °C). IR (KBr) 1617 cm^{-1}. MS *m*/*z* 664 ($[M + H]^+$). HRMS (FAB) found *m*/*z* 663.0681 (M^+); calcd for $C_{32}H_{28}CuN_2O_6S_2$ ($[M + H]^+$) 664.0763. Elemental Anal. calcd for $C_{32}H_{28}CuN_2O_6S_2$: C, 57.86; H, 4.25; N, 4.22. Found: C, 57.13; H, 4.34; N, 4.01.

Complex 9b. This complex was prepared by similar procedures except using $Ni(OAc)_2 \cdot 4H_2O$ with a yield of 67% red-brown solid, mp >250 °C. ^1H NMR (300 MHz, $CDCl_3$) δ 7.57 (dd, 2H, $J = 2.5$ and 9 Hz), 7.39 (d, 2H, $J = 2.5$ Hz), 7.37 (s, 2H), 7.02 (d, 2H, $J = 9$ Hz), 6.16 (s, 2H), 4.26−4.20 (m, 8H), 3.50 (br, 2H), 2.39−2.35 (m, 2H), 1.74−1.80 (m, 2H), 1.52−1.48 (m, 2H), 1.43−1.38 (m, 2H). The poor solubility of this compound prevented characterization by ^{13}C NMR. IR (KBr) 1614 cm^{-1}. MS *m*/*z* 659 ($[M + H]^+$). HRMS (FAB) found *m*/*z* 658.0732 (M^+); calcd for $C_{32}H_{28}N_2NiO_6S_2$ ($[M + H]^+$) 659.0821. Elemental Anal. calcd for $C_{32}H_{28}N_2NiO_6S_2$: C, 58.29; H, 4.28; N, 4.25. Found: C, 57.97; H, 4.42; N, 4.01.

Electrochemistry. Electrochemical studies were performed under an air-free drybox using a one-compartment cell with either a platinum button or 5 μm interdigitated microelectrode as the working electrode, a platinum coil counter electrode, and an isolated Ag/Ag^+ reference electrode. The electrolyte solutions used for all electrochemistry and conductivity measurements were 0.1 M $^nBu_4NPF_6$ in CH_3CN. All electrochemical potentials are reported to the ferrocene/ferrocenium (Fc/Fc^+) redox couple. Films on interdigitated microelectrodes for conductivity studies were grown at a constant potential slightly more positive than the monomer oxidation potential. Once grown, the films were rinsed with fresh electrolyte and placed in a monomer-free solution. Drain current measurements were typically run a 2 mV/s with a 40 mV offset potential between the two working electrodes. Film thicknesses were determined with a Tencor P10 Surface Profilometer. The minimum thickness was used to calculate the conductivity (σ) of the film.

In Situ EPR. Films for in situ EPR studies were prepared on a platinum wire working electrode, a platinum wire counter electrode, and a silver wire quasireference electrode (externally referenced to ferrocene) by polymerization of a monomer solution in a 10 mL graduated cylinder. The polymer was then transferred to a quartz EPR-electrochemistry cell obtained from Wilmad Glass containing a 0.1 M $^nBu_4NPF_6$/MeCN electrolyte solution. Spectra were obtained using a Bruker Model EMX Electron Paramagnetic Resonance Spectrometer operating at X-band with 100 kHz field modulation at room temperature. Microwave powers of 100 mW were used. Magnetic fields were measured with a Hall field probe with microwave frequencies in the 9 GHz range. The resulting EPR spectra were analyzed using WinEPR software from Bruker. Spectra were taken at various points during the CV to ensure that the EPR signal width remained constant. In this case, the maximum EPR signal intensity was followed as a function of oxidation potential while scanning the polymer through a complete system at 10 mV/s. In cases where the signal width varied, EPR spectra were taken of the polymer film in 50 mV intervals and the data were plotted as the second integral of the signal versus oxidation potential.

Spectroelectrochemistry. In situ spectroelectrochemical measurements were performed with a home-built spectroelectrochemical cell using an ITO working electrode (100 Ω/square), a platinum wire counter electrode, and silver wire reference electrode. Films were grown under a nitrogen atmosphere, after which the compartment was washed 3 times with fresh electrolyte and then filled with fresh electrolyte and then a CV was run. The cell was then transferred to the UV−vis spectrophotometer and spectra were taken at 100 mV intervals from the fully reduced form to the fully oxidized form of the polymer. In certain cases, the reversibility of the system was interrogated by taking spectra during the reduction scan.

Acknowledgment. The authors would like to thank the Office of Naval Research for funding. This work made use of MRSEC Shared Facilities supported by the National Science Foundation under Award No. DMR-9400334. R.P.K. would like to thank Professor Daniel Nocera for helpful discussions.

JA991285M